Pore pressure evolution in bed sediment overridden by debris flow: A general formulation

Pore pressure evolution in bed sediment overridden by debris flow: A general formulation

Hongchao Zheng[1], Zhenming Shi[1], Kevin J Hanley[2], Yuanyuan Zhou[1*], Xinli Hu[3]

[1]Department of Geotechnical Engineering, College of Civil Engineering, Tongji University, China

[2] School of Engineering, Institute for Infrastructure and Environment, The University of Edinburgh, United Kingdom

[3] Faculty of Engineering, China University of Geosciences, China

Corresponding author: Yuanyuan Zhou, 1710017 @tongji.edu.cn

Abstract

Debris flows can grow dramatically in volume and mobility as they override bed sediment due to the reduction in bed-friction resistance caused by high pore-fluid pressure (PP). However, the mechanisms that control PP evolution in overridden bed sediment are still unclear. Here, a new mathematical model clarifies how diverse styles and magnitudes of PP evolution can result from regulation of the flow diffusion and shear contraction of bed sediment. Normalization of the model equations shows that the propensity for PP generation depends on timescales of PP diffusion and deformation of the bed grains. The PP of saturated bed sediment under immobile conditions is equal to the fluid pressure at the bottom of the flow due to a non-flux basal boundary. However, the PP of unsaturated bed sediment is lower than that of the overlying flow. PP diffusion from a debris flow into an unsaturated bed increases with

the bed's permeability and water content. The shear deformation behavior changes from undrained to drained with increasing permeability or decreasing shear velocity of the saturated bed sediment, leading to a reduced magnitude of pore pressure. By contrast, the shear deformation transitions from drained to undrained behavior with increasing permeability and water content of unsaturated bed sediment. The entrainment rate and erosion pattern of bed sediment are closely related to the PP evolution and liquefaction ratio of the bed sediment due to Coulomb-friction shear tractions. Our models can be used to interpret the feedback of PP on the flow momentum during debris-flow entrainment.

Keywords: debris flows, pore pressure, bed sediment, shear deformation, erosion pattern

1. Introduction

Debris flows are common phenomena in mountainous regions worldwide (e.g., Iverson, 1997; de Haas and van Woerkom, 2016; Zheng et al., 2018, 2022; Chen et al., 2021). They often occur in steep gullies when landslides and loose debris initiate, driven by gravity (e.g., Iverson, 1997; Pudasaini, 2012; Wang et al., 2020). Debris flows rush down mountainsides and spill onto valley floors where they can block rivers, cover floodplains and deteriorate the regional ecological environment (e.g., Iverson et al., 2011; de Haas et al., 2015; Zheng et al., 2021a, b).

Researchers have long recognized that debris flows can gain much of their volume and destructive power by side collapse and basal erosion in the flow process (e.g., Pierson, 1980; Takahashi et al., 1992; Iverson, 1997; Hungr et al., 2005). Debris flows have been observed to increase in volume by several orders of magnitude before deposition on flatter terrain downstream (Breien et al., 2008; Navratil et al., 2013; Theule et al., 2015). For instance, volumetric increases of 50 times the initial volume and volumetric growth rates exceeding 20 $m^3\ m^{-1}$ have been reported (Hungr et al., 2005; Santi et al., 2008). The debris flow in Wenjia Gully increased threefold in volume and the volume of bed sediment entrained by the flow reached 5×10^7 m^3 (Tang et al., 2012). Despite their ubiquity and potentially hazardous impact, the mechanisms that govern erosion rate and pattern of debris flows are still unclear, hampering efforts to evaluate and predict the areas endangered by debris flows (Scheidl and Rickenmann, 2010; Iverson et al., 2011; Mangeney, 2011; Zheng et al., 2021c). Recently, the erosion mechanisms of debris flows have been comprehensively

explored by Iverson and Ouyang (2015), An et al. (2021), as well as Pudasaini and Krautblatter (2021).

Abundant field and laboratory studies have been conducted to analyze the effects of flow composition and watershed terrain on the erosion potential (e.g., Hungr and Evans, 2004; Hsu et al., 2008; Berger et al., 2010, 2011; Iverson, 2012; de Haas and van Woerkom, 2016). Although these variables have an influence, debris-flow erosion is inherently regulated by the interaction between the bed sediment (BeS) and overlying flow (Iverson, 2012). However, the feedback of the underlying BeS on the erosion process is critical. Iverson et al. (2011) conducted large-scale experiments with sediments overridden by debris flows and found that significant entrainment occurs only if a large pore fluid pressure (PP) develops in wet BeSs. Thus, it is meaningful to understand the mechanisms that control PP evolution of BeS.

Little consensus has emerged regarding the erosion pattern of debris flows. Progressive scour in the form of incorporating the BeS grain by grain and mass movement of parts of the BeS are the patterns observed experimentally by de Haas and van Woerkom (2016). According to Takahashi (2007) and McCoy et al. (2012), en masse failure is defined as the BeS is entrained along the bedrock–sediment interface. Failure of parts of the BeS is considered to follow a slab-by-slab manner in which the erosion front moves from the flow–bed interface down via multiple failures with thicknesses of many particle sizes, but with depths smaller than the total BeS thickness (McCoy et al., 2012). This progressive slab-by-slab failure is described as mass movement by Iverson et al. (2011) and Zheng et al. (2021c). En masse failure

can be considered as mass movement according to Iverson et al. (2011). Thus, the erosion patterns of debris flows can be classified as progressive grain-by-grain scour or mass movement (Fig. 1). In this study, “erosion”, “entrainment” and “scour” are synonymous, meaning that BeS is carried away by the overlying flow.

Field observations in Chalk Cliffs basin show that BeS is entrained by mass movement without observing en masse failure (McCoy et al., 2012). In contrast, the volume of debris flows in San Gabriel Mountains is bulked by en masse failure (McGuire et al., 2017). Actually, the erosion process of debris flow is complicated and dependent on the catchment. These two erosion patterns can occur during debris-flow transportation. Laboratory model experiments indicate the erosion pattern is closely related to the grain composition of the BeS (Zheng et al., 2021c). However, the effect of grain composition of bed sediment on the emergence of different erosion patterns requires further clarification.

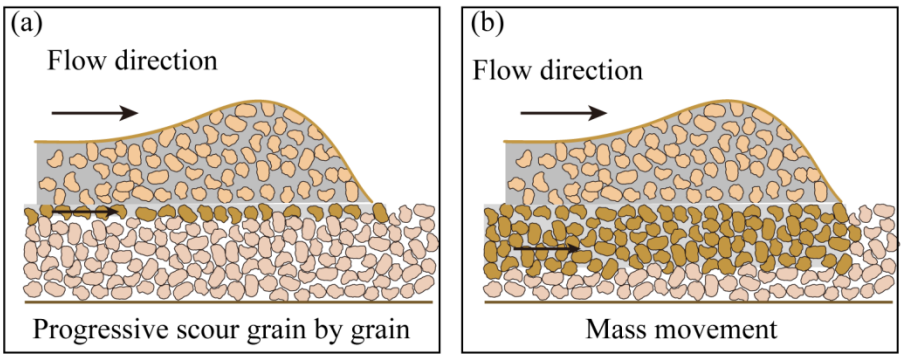

Figure 1. Schematic views illustrating the erosion pattern by which debris flows might entrain sediment: (a) progressive grain-by-grain entrainment; (b) mass movement of multiple grain layers. Dark grains within the BeS are entrained by debris flow.

The saturation of natural BeS depends on rainfall intensity and duration (Berti and Simoni, 2005). BeS can be completely saturated from surface runoff and

groundwater. However, the water content of BeS is usually far from saturation when these beds are capable of draining the rain water infiltrating from the surface. The characteristics of debris flows and erosion rates are affected by the saturation degree of the BeS. A growing flow velocity and a high erosion rate are observed for BeSs with a large saturation degree, but they diminish for relatively dry BeSs (Iverson et al., 2011; Reid et al., 2011; McCoy et al., 2012). This is because high PP developed in wet BeS reduces basal friction of flow, and facilitates the erosion of the BeS. Analogously, it has been observed that the erosion rates of widely graded BeSs are lower than those of coarse-grained BeSs because coarse-grained BeSs with higher permeability are favorable to PP development (Zheng et al., 2021c). The response mechanisms of PP in saturated and unsaturated BeSs overridden by debris flows remain an open question.

The diverse outcomes of experiments and field measurements with debris flows indicate the basic physics regarding how PP evolves in response to general deformation of BeS are still unclear. An expected universal theory should be able to explain experimental and field observations and link existing models. It should also address some fundamental questions: Can PP developed in BeS containing coarse sand with high permeability be greater than that in BeS containing fines with low permeability (Gabet and Mudd, 2006; Zheng et al., 2021c)? What is the difference between PP feedback of saturated and unsaturated BeSs overridden by debris flows (McCoy et al., 2012)? How does the water content of BeS regulate PP evolution (Iverson et al., 2011)?

In order to address these questions, we develop a theoretical model within the scope of shearing and immobile BeSs, where the pore fluid diffuses into this bed and bed grain deformation is neglected. Applying the theory to general PP response cases allows derivation of the propensity for pore-fluid pressurization of saturated and unsaturated BeSs, validated by experimental and field data. The behavior of BeSs during entrainment is used to interpret the mechanisms that control PP evolution.

The manuscript is organized as follows. We develop a formulation based on mass and momentum conservation for the general PP response to entrainment by debris flow in section 2. This formulation is not restricted to a particular type of BeS and can be used to study both immobile and shearing beds under saturated and unsaturated conditions. To investigate the effects of the water content of the BeS on the PP behavior, sections 3 and 4 describe PP evolutions of saturated and unsaturated BeSs, respectively, overridden by debris flows. In section 5, we discuss the differences in PP behavior of saturated and unsaturated BeSs, infer the correlation between liquefaction ratio of the BeS and erosion patterns of progressive grain-by-grain entrainment and mass movement, and analyze the propagation of fluctuating PP by considering fluctuation frequency and BeS diffusion. We present our conclusions in section 6. In Appendix A the pore pressure diffusion equation is developed by mass and momentum conservation laws. In Appendix B we show PP evolution versus the dilation rate caused by compressibility of the BeS and changes in mixture shear strains. In Appendix C we derive the infiltration depth of unsaturated BeS based on the Green–Ampt model during flow loading.

2. Theoretical model

Based on mass conservation and Darcy laws, a pore pressure diffusion equation describing the temporal and spatial evolution of the PP in response to flow loading is derived in Appendix A

$$\frac{dP}{dt} = \nabla \cdot \frac{k}{C\mu} \nabla P + \frac{d\sigma}{dt} - \frac{\dot{\gamma} \tan \varphi}{C} \tag{1}$$

where P is the excess (over hydrostatic) fluid pressure and σ is the total normal stress; k is the permeability of the BeS and μ is the viscosity of pore fluid; t is the time and $\dot{\gamma}$ is the shear rate of the BeS; φ is a dilatancy angle that describes the tendency of the bed grains to contract ($\varphi < 0$) or dilate ($\varphi > 0$). C is the drained compressibility of the bulk BeS.

A non-dimensional analysis is performed for investigating the relative magnitude of different terms in Eq. (1). The characteristic magnitudes of the variables in Eq. (1) are defined as $P = \hat{P}/C,\ t = \hat{t}t_0,\ \sigma = \hat{\sigma}/C,\ \dot{\gamma} = \hat{\dot{\gamma}}/t_0$ where ^ notation represents non-dimensional variables, and t_0 is the timescale factor.

Two derivatives are included in the second term of Eq. (1). The first divergence arising from Eqs. (A4) and (A5) denotes particle-scale movement. Thus, the derivatives in these operators are scaled by d_g^{-1}, a characteristic particle diameter, and $\nabla \cdot = \hat{\nabla}_1 \cdot /d_g$ (Goren et al., 2010). However, the gradient operator derived in Eq. (A7) denotes a larger length scale, which is applicable for Darcy law. Therefore, the derivatives in this operator are scaled by l^{-1}, a length scale of PP diffusion and $\nabla \cdot = \hat{\nabla}_2 \cdot /l$. A natural choice for l is $\sqrt{Dt_0}$, where $D = k/(C\mu)$ is the diffusion coefficient of the PP, and $t_0 = d_g/u_0$ is the timescale of particle deformation, where

u_0 is the velocity of sediment grains.

Assigning these non-dimensional variables to Eq. (1) results in

$$\frac{d\hat{P}}{d\hat{t}} = \frac{D}{lu_0}\hat{\nabla}_1\left(\hat{\nabla}_2\hat{P}\right) + \frac{d\hat{\sigma}}{d\hat{t}} - \hat{\dot{\gamma}}\tan\varphi \tag{2}$$

The coefficients of the second term in Eq. (2) can be expressed as a function of a Deborah number:

$$\frac{D}{lu_0} = \sqrt{\mathrm{De}_d^{-1}} \tag{3}$$

The Deborah number, $\mathrm{De_d} = t_d/t_0$, is defined as the ratio of a relaxation timescale to a characteristic process timescale (Osswald, 1998). Here, the relaxation timescale, $t_d = d_g^2/D$, is the timescale for pore-pressure diffusion across a single particle and the characteristic process timescale, t_0, is the timescale of particle deformation.

The combination of Eqs. (2) and (3) yields

$$\frac{d\hat{P}}{d\hat{t}} = \sqrt{\mathrm{De_d^{-1}}}\hat{\nabla}_1\left(\hat{\nabla}_2\hat{P}\right) + \frac{d\hat{\sigma}}{d\hat{t}} - \hat{\dot{\gamma}}\tan\varphi \tag{4}$$

It shows that the evolution of PP in a Lagrangian frame of reference is related to the diffusivity and two types of forces. One arises from increasing flow loading (third term) and the other involves PP modification due to shear-induced bed dilation (fourth term).

In the analysis, we aim to study the effects of the permeability and shearing behavior of the BeS in saturation and unsaturation on the evolution of PP. For this purpose, it is necessary to specify another Deborah number, $\mathrm{De}_\zeta = t_\zeta/t_0$, which expresses the ratio between $t_\zeta = h^2/D$, the timescale of PP diffusion over a saturated BeS, and t_0, the timescale of particle deformation. The non-dimensional pore-pressure

diffusion equation of BeS is expressed as

$$\frac{d\hat{P}}{d\hat{t}} = \sqrt{\mathrm{De}_\zeta^{-1}}\,\hat{\nabla}_1\left(\hat{\nabla}_2\hat{P}\right) + \frac{d\hat{\sigma}}{d\hat{t}} - \hat{\dot{\gamma}}\tan\varphi \tag{5}$$

As shown in Fig. 2, we consider a debris flow to pass across an erodible BeS overlying an immobile bed with a non-flux boundary. For a fully saturated BeS during debris-flow entrainment, depth of PP diffusion h refers to the depth of the erodible bed H. That is, PP cannot diffuse below the erodible bed. De_ζ of a saturated BeS is expressed as

$$\mathrm{De}_\zeta = \frac{H^2}{Dt_0} \tag{6}$$

For an initially unsaturated BeS, h is the infiltration depth h_i in the normal direction during a deformation timescale t_0 (Fig. 2b). According to the Green–Ampt model (Green and Ampt, 1911; Chen and Young, 2006), h_i is approximated as (see the deduction in Appendix C)

$$h_i = f(\theta) = \frac{Kt_0}{\theta} \tag{7}$$

where $K = \dfrac{k\rho_f g}{\mu}$ is the saturated hydraulic conductivity in the saturated zone above the wetting front. ρ_f is the mass density of the pore fluid and g is the acceleration due to gravity. $\theta=\theta_s-\theta_i$ is the difference between the saturated water content θ_s and initial water content θ_i of the BeS. Here, θ_i of the unsaturated BeS is assumed to be uniform in the depth direction. Hence, De_ζ of the unsaturated BeS is

$$\mathrm{De}_\zeta = \frac{K^2 t_0}{\theta^2 D} \tag{8}$$

The diffusive dissipation of PP in Eq. (5) depends on De_ζ. When $\mathrm{De}_\zeta \le 1$, the

diffusive dissipation of the PP is significant and the deforming BeS behaves as well drained. The effects of shearing and compression of the BeS on PP evolution depend on their rates relative to the rate of diffusive dissipation of the PP (Iverson, 1997; Goren et al., 2010). On the contrary, nearly undrained behavior of the BeS is described in Eq. (5) when $De_\zeta \geq 1$. In this situation PP changes instantaneously and uniformly in response to the shear deformation or compressional loading of the BeS that causes pore-volume changes (Iverson, 2012). PP related to undrained behavior normally has a higher magnitude than that of well-drained BeSs under the same rates of shear and loading (Goren et al., 2010). The process of undrained loading of torrent deposits has been reported by Hutchinson and Bhandari (1971) for earth flows. Sassa (1985) introduces the processes of undrained shear of BeSs overridden by debris flows accompanied by high PP generation.

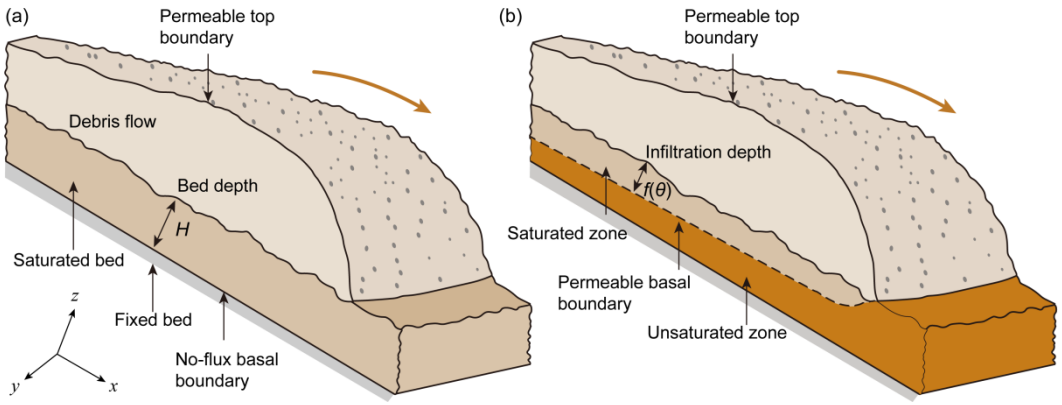

Figure 2. Schematics illustrating the erosion of a BeS by debris flows modified from Iverson (2012). (a) Saturated BeS. Non-flux boundary is located at the bottom of the saturated BeS. (b) Unsaturated BeS. A permeable boundary is located at the wetting front between an upper saturated zone and a lower unsaturated zone, where the water content is kept at the initial value. The bed rock in the gully is usually considered as

the fixed bed. The depth of the erodible sediment layer H is the thickness of loose debris deposited on the bed rock.

3. Pore-pressure evolution of saturated bed sediment

The PP evolution within immobile and shearing saturated BeSs subjected to loading by a debris flow is investigated. An immobile BeS is one in which the bed grains remain static when debris flows override the BeS, i.e., a fixed bed (Fig. 3a). This situation arises for debris flows with a small volume and low flow depth, exerting a weak shear stress τ_f to carry away the BeS and a low loading to compress the BeS. That is, $\nabla \cdot \mathbf{u}_s = 0$ in Eq. (A6) and the pore volume remains unchanged. If shearing were to occur without a volume change of the BeS, then Eq. (A8) reduces to $\dot{\gamma} \tan\varphi = C \frac{d\sigma_e}{dt}$. This indicates that σ_e would decrease or increase with time if the shearing proceeds with $\varphi < 0$ or $\varphi > 0$, respectively, until a critical state (steady state) is achieved. Compared with immobile BeS, a shearing BeS means that $\nabla \cdot \mathbf{u}_s \neq 0$ in Eq. (A6) and the PP of BeS changes during entrainment (Fig. 3b). Here, a shearing BeS refers to a bed that is sheared or compressed by a debris flow.

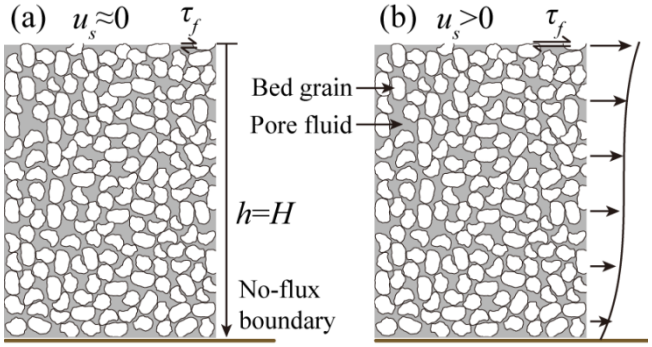

Figure 3. Saturated bed sediments entrained by debris flow: (a) immobile; (b) shearing. The depth of PP diffusion h is the depth of the erodible bed H due to the

non-flux bottom boundary. u_s is the shear velocity of sediment grains.

3.1 Immobile bed sediment

PP would not be generated by saturated bed grains with no or negligible volume changes during entrainment. When the velocity of bed grains in the shearing layer is low and the shear displacement is too small to generate much contraction, a negligible PP is generated. For example, data from laboratory ring shear tests with landslide soil specimens of 7 cm thickness indicate the critical shear displacement to generate a considerable dilatancy is approximately 0.1 m (Iverson, 2000).

PP of a debris flow transmits into the entire BeS at subsonic speeds (Iverson and LaHusen, 1989; McCoy et al., 2012) when the pores in the flow and the bed become connected. PP within the BeS approaches the basal fluid pressure of debris flow. This PP is distributed uniformly in depth due to a non-flux basal boundary of the BeS (Fig. 3a). The evolution of the basal fluid pressure of a debris flow on a fixed bed is associated with the granular dilation rate and diffusion timescale of debris flow. It has been derived by Iverson and George (2014) and is not discussed here.

3.2 Shearing bed sediment

The values of De_ζ can vary widely, affected by u_0, H and k for saturated BeS inferred from Eq. (6). The values of u_0 vary from 10^{-6}–10^{0} m/s, referring to Iverson (2012). k also has a wide range, from 10^{-12} m^2 for silty sand to 10^{-9} m^2 for gravel. The grain-size distribution of loose debris sediments is regulated by the lithology of bedrock in their basins (Tiranti et al., 2008). Silty clay with a permeability as small

as 10^{-17} m^2 is rarely reported in areas endangered by debris flows. K values are estimated to be 1×10^{-2} m/s, 1×10^{-3} m/s and 1×10^{-4} m/s for gravel, sand and silty sand, respectively (Iverson, 2012). For gravel, the values of D measured by laboratory tests have a magnitude of 10^{-3} m^2/s (de Haas et al., 2015; Kaitna et al., 2016). Considering that the values of drained compressibility C are approximately 10^{-6} Pa^{-1} for different BeSs (Iverson et al, 2012), D values are determined to be 10^{-4} m^2/s and 10^{-5} m^2/s for sand and silty sand, respectively (Major, 2000).

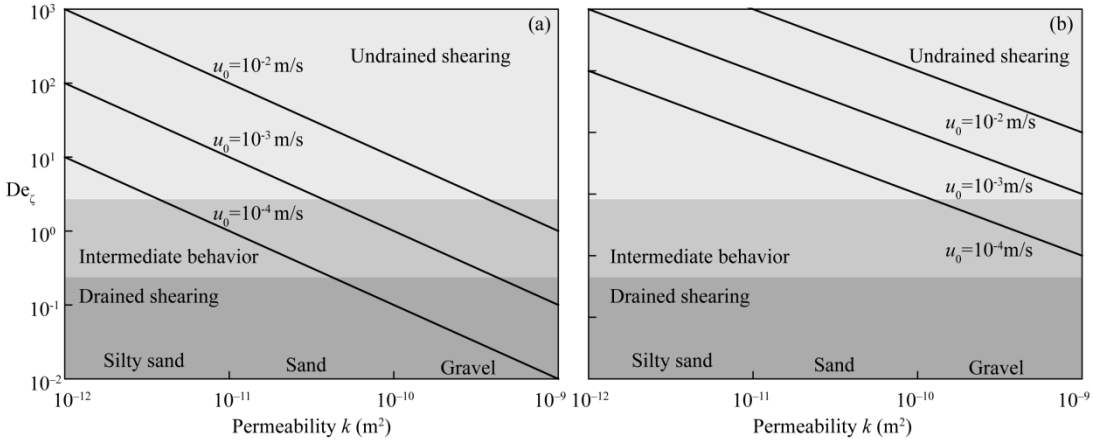

Figure 4. Relationship between the parameter De_ζ and permeability k for a range of velocities of sediment grains v calculated from Eq. (6). Depths of the erodible bed H are 0.01 m and 0.1 m in panels (a) and (b), respectively. Labels along the horizontal axis identify types of sediments typically exhibiting these k values (Iverson, 2012). Grey regions identifying the ranges of De_ζ values imply that shear behavior can be characterized as “drained,” “intermediate”, or “undrained.”

As shown in Fig. 4, a significant PP can be generated by slight shear displacements of the saturated bed composed of silty sand or sand during entrainment of a debris flow. $De_\zeta>1$ is suitable for u_0 with a magnitude as small as 10^{-4} m/s for H = 0.1 m. In particular, the depth of erodible bed H can be several meters for

catastrophic debris flows with high basal shear stress. In this situation, the saturated BeSs present effectively undrained behavior according to Eq. (5) and the second diffusion term is approximately zero. The average PP is then approximated as

$$P(t) = \sigma - \frac{1}{C}\int_0^t \dot{\gamma}\tan\varphi \tag{9}$$

The flow loading in the second term is borne by the pore fluid within the BeS. Moreover, pore fluid is pressurized by the shear contraction indicated by the third term in Eq. (9). The high PP induced by destruction of the bed-soil structure instigates the incorporation of loose deposits into moving debris flows (Sassa and Wang, 2005). By contrast, $De_\zeta \leq 1$ applies if gravel or coarser debris is present in a bed overridden by a debris flow with a low u_0 and a small H (Fig. 4a). Indeed, drained behavior of the shear deformation is effectively presented and weak PP is likely to generate due to the high diffusivity of coarse debris. Eq. (5) reduces to

$$\nabla \cdot \frac{k}{C\mu}\nabla P = -\frac{d\sigma}{dt} + \frac{\dot{\gamma}\tan\varphi}{C} \tag{10}$$

PP diffusion originates from the flow loading and bed shear deformation. The dynamic fluid pressure gradient depends linearly on solid velocity (Eq. (A7)). In this case, the PP of the saturated BeS is significantly affected by the basal fluid pressure of a debris flow. BeS presents a PP behavior analogous to those of immobile BeSs described in section 3.1. In addition, with $\mathrm{De}_\zeta \approx 1$, an intermediate behavior that is not categorizable solely as undrained or drained is possible.

4. Pore-pressure evolution of unsaturated bed sediment

In this section, we investigate the PP evolution within unsaturated immobile and

shearing BeSs during loading by debris flows. An unsaturated BeS is divided into an upper saturated zone due to flow infiltration and a lower unsaturated zone where the water content maintains an initial value (Fig. 5). The interface between both zones is termed the wetting front. Air in pores below the wetting front is likely to be displaced by overlying water (Iverson et al., 2011). As a result of the high compressibility of the pore air, the wetting front is considered as a permeable boundary for the excess PP.

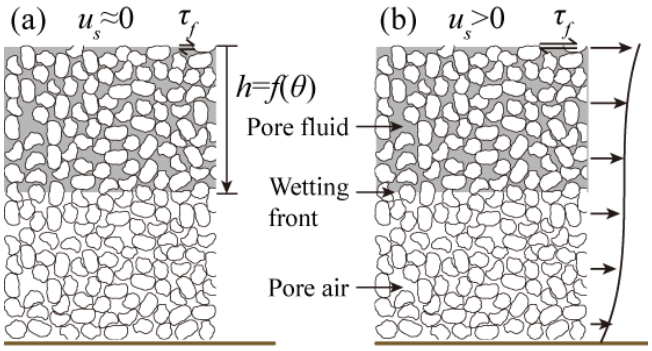

Figure 5. Unsaturated bed sediments entrained by debris flow: (a) immobile; (b) shearing. The depth of PP diffusion h is the infiltration depth h_i indicated by Eq. (7).

4.1 Immobile bed sediment

With $\nabla \cdot \mathbf{u}_s = 0$ for an immobile BeS, Eq. (1) reduces to the standard constitutive equation used for analysis of compressibility in soil consolidation theories (Terzaghi, 1943). It is useful to divide the PP at the bottom of a debris flow, P_e, into two components:

$$P_e = P_u + P_w \tag{11}$$

where P_u is the PP diffused from the top of the debris flow (Fig. 2b), and P_w is the PP diffused from the wetting front of the BeS. An expression for one-dimensional diffusion of P_w is given by

$$\frac{\partial P_w}{\partial t} = D\frac{\partial^2 P_w}{\partial z^2} \tag{12}$$

The transient excess PP, P_i, within the saturated zone for a permeable boundary at the bottom is given by (Major, 2000)

$$P_i(z,\ t) = 8P_w \sum_{n=0}^{\infty} \frac{1}{(2n+1)^2\pi^2} \cos(\lambda_n) e^{-\lambda_n^2 \frac{Dt}{h_i^2}} \tag{13}$$

where the eigenvalues λ_n are defined as $\lambda_n = \frac{(2n+1)\pi}{2}$.

Substitution of Eq. (7) into Eq. (13) during the timescale of flow infiltration t_i yields

$$P_i(z,\ t_i) = 8P_w \sum_{n=0}^{\infty} \frac{1}{(2n+1)^2\pi^2} \cos(\lambda_n) e^{-\lambda_n^2 \frac{D\theta^2}{K^2 t_i}} \tag{14}$$

The value of θ varies between 0–0.4 for natural loose sediments (Iverson et al., 2011). When θ=0, the BeS is fully saturated and the excess PP at the flow bottom cannot diffuse from the BeS. In this case, it behaves the same as the saturated BeS in an immobile condition.

An exemplified solution to Eq. (12) using typical material values is plotted in Fig. 6. Here, values of θ are taken as 0.1, 0.2 and 0.4 for the unsaturated BeS. The infiltration time t_i is determined to be 1 second. The depth of the PP diffusion in the BeS under an immobile condition is largely affected by permeability and water content. The infiltration depth h_i increases with increasing permeability of the BeS, contributing to a growth of the diffusion timescale t_ζ and a reduction in the diffusion rate in Eq. (5). When θ=0.4, h_i is 1.25×10^{-1} m for gravel, decreasing to 1.25×10^{-3} m for silty sand. The penetration depth of the PP in silty sands is limited to the grain diameter of the sand and the PP of debris flows rapidly dissipates from the wetting

front at the bottom. In contrast, the depth of the PP penetration is larger than a dozen centimeters for gravel and the dissipation from the wetting front is relatively low. In addition, t_ζ rapidly decreases with increasing θ and thus enhances the dissipation of the PP in Eq. (13), considering h_i is inversely proportional to θ. This indicates that the depth of the PP diffusion in a wet BeS is higher than that of a dry BeS.

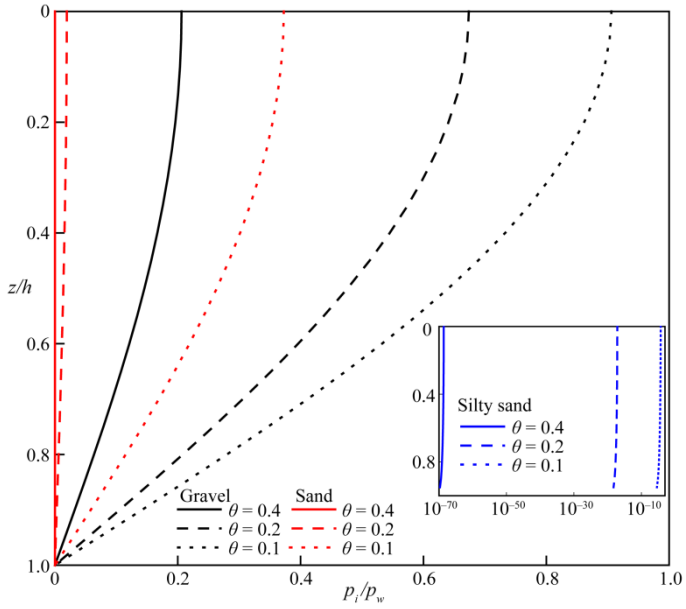

Figure 6. Depth profiles of excess PP within the saturated zone resulting from debris flows applied at the interface between the flow and BeS. K values are 5×10^{-2} m/s, 5×10^{-3} m/s and 5×10^{-4} m/s for gravel, sand and silty sand, respectively. The corresponding D values are determined to be 1×10^{-2} m^2/s, 1×10^{-3} m^2/s and 1×10^{-4} m^2/s, respectively. As the permeability and water content of the bed sediment increase, the depth to which the excess PP penetrates into the bed increases.

4.2 Shearing bed sediment

Two scenarios exist in a shearing BeS depending on the relative depths between of flow-infiltration induced wetting front and the shearing layer driven by overlying

flow during the timescale of grain deformation (Fig. 7). In the first case, the infiltration depth is larger than the thickness of the shearing layer. It is applicable to sediments like gravel soils with a high permeability and a large infiltration depth. The PP induced by the shearing contraction of bed grains diffuses within the entire saturated zone. The shear rate $\dot{\gamma}$ in Eq. (5) is considered as the mean shear rate within the saturated zone. For field measurements of debris flows carried out by McCoy et al. (2012), penetration of the wetting front into the BeS coincided with or preceded entrainment. In the other case, the wetting front is located within the shearing layer. PP induced by shear deformation of unsaturated sediments is negligible. Thus, the generation and diffusion of PP are limited to the zone above the wetting front. Sediments like silty soils with a low permeability and a small infiltration depth fit this scenario.

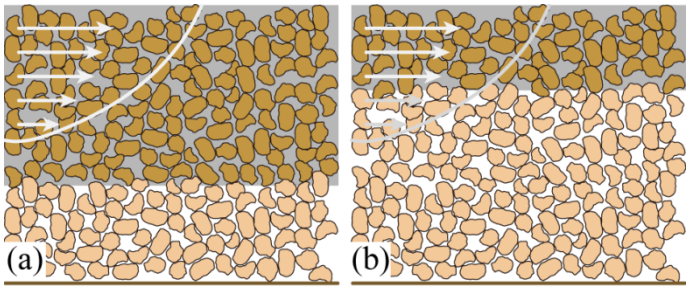

Figure 7. Relationship between the infiltration depth and shearing layer: (a) depth of the shearing layer is smaller than the infiltration depth; (b) depth of the shearing layer is larger than the infiltration depth. Curves and arrows in light gray depict the shearing deformation of BeS overridden by debris flows. The dark gray zone indicates the saturated zone caused by flow infiltration.

When $De_\zeta<1$, PP can easily diffuse from the shearing layer to the boundaries

within the timescale of deformation, displaying drained behavior according to Eq. (5). In contrast, when $De_\zeta > 1$, the PP diffusion front originating along the shearing layer does not reach the boundaries within the timescale of deformation and undrained behavior is observed. When $De_\zeta \approx 1$, an intermediate behavior that is not categorizable solely as drained or undrained may appear.

De_ζ of a shearing unsaturated BeS increases with increasing permeability k and initial water content θ_i (Fig. 8). For a dry BeS (θ=0.4), $De_\zeta < 1$ and the behavior of silty sands and sands is dominated by drained shearing, hence the propensity to generate excess PP is weak. In this case, the PP of the BeS is significantly affected by the basal PP of debris flows. The BeS presents a PP evolution behavior similar to that of immobile BeSs described in section 4.1. Undrained behavior is only observed for gravels. As the water content increases, the shearing layer composed of sands and gravels transitions from drained to undrained shearing behavior. The magnitude of the PP generation is thus enhanced. Undrained shearing behavior does not present for silty sands even for θ=0.1. According to large-scale experiments conducted by Iverson et al. (2011), for initial water contents $\theta_i > 0.22$, PPs of wet BeSs increase from 0 to nearly lithostatic values in a short time when the sediment is overridden by debris flows. However, the PP responses to flow loading are much smaller when $\theta_i < 0.22$. This situation is also consistent with the observations of debris flows at Chalk Cliffs where the PP of wet BeSs is significantly higher than that of dry BeSs (McCoy et al., 2012).

The tendency to generate high PPs in gravels is stronger than in silty sands. This

is coherent with laboratory observations revealing significant PPs are developed in coarse-grained BeSs but a weak PP appears in widely graded BeS although the former has a lower θ_i than the latter (Zheng et al., 2021c). Gabet and Mudd (2006) further find a correlation between debris flow mobilization and fines/sands ratio. They suggest that soils with a small fines/sands ratio are mobilized due to their high permeability allowing rapid fluid inflow and PP gain that lead to a second sliding phase and a longer sliding distance.

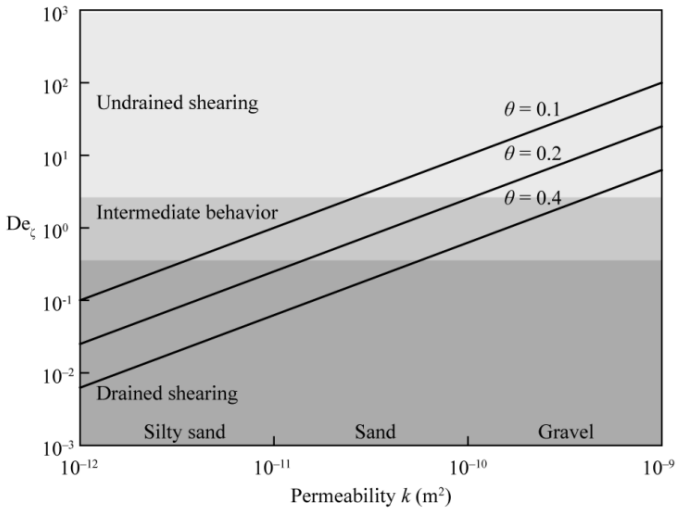

Figure 8. The relationship between the parameter De_ζ and permeability k for a range of water contents θ calculated from Eq. (8). Grey regions identifying the ranges of De_ζ values imply that the shear behavior can be categorized as “drained,” “intermediate”, or “undrained.”

5. Discussion

We first discuss the differences in PP behavior of saturated and unsaturated BeSs versus their permeability. Then, we infer the correlation between liquefaction ratio of the BeS caused by PP evolution and erosion patterns of progressive entrainment and

mass movement. Finally, fluctuating PP propagation in the BeS is analyzed considering fluctuation frequency and BeS diffusion.

5.1 Shearing behavior of saturated and unsaturated bed sediments

Regardless of saturated or unsaturated BeSs, the propensity to generate PP increases with increasing shear velocity of debris grains. This is in accordance with the PP evolution of moving rod arrays in saturated conditions (Iverson, 1993; Goren et al., 2010):

$$P = -\frac{\mu H}{k} u_s \tag{15}$$

where u_s is the shear velocity of sediment grains.

Undrained shearing behavior tends to transition to drained shearing behavior as permeability increases when the saturated BeS is overridden by a debris flow (Fig. 9). The magnitude of induced PP in Eq. (15) is reduced as the permeability of the BeS increases. The reason is that the diffusion D of the PP in Eq. (6) is enhanced by the permeability gain, resulting in a reduction in Deborah number, De_ζ, in Eq. (5). Silty sands therefore tend to have undrained shear behavior and have a higher PP than gravels. In contrast, drained shearing behavior transitions to undrained shearing behavior with increasing permeability when an unsaturated BeS is eroded by a debris flow. The infiltration depth of flow and diffusion depth of PPs are linearly correlated with the permeability in Eq. (7), lowering the diffusion of the PP. The magnitude of the PP developed in unsaturated BeSs in Eq. (5) is thus fortified by permeability. As a result, silty sands barely show an undrained shearing behavior and have a smaller PP than gravels.

An unsaturated BeS can become saturated when the wetting front reaches the bottom of the movable bed during the timescale of grain deformation. This situation can occur if the BeS is highly permeable, i.e., with a large initial water content, or if its thickness is relatively small. Simultaneously, the shearing behavior of the BeS changes from unsaturated to saturated. The magnitude of PPs is thus enhanced due to the non-flux boundary at the bottom of the saturated BeS. This is obtained by comparing the magnitudes of De_ζ in Fig. 9, showing the propensity for shearing deformation to generate PP.

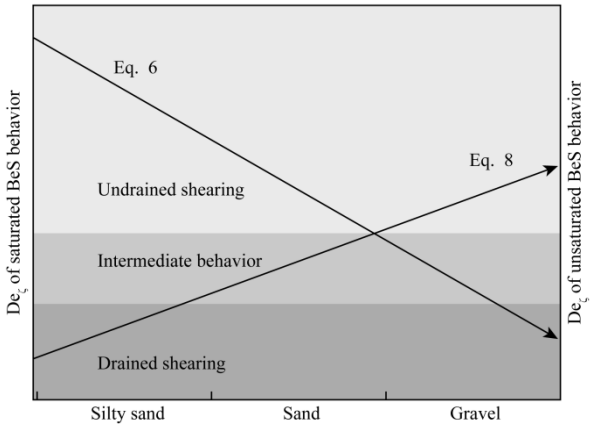

Figure 9. Behavior of the PP in saturated and unsaturated BeSs as a function of permeability. Saturated BeSs present a transition from undrained to drained shearing behavior with the increase of permeability indicated by Eq. (5). In contrast, an inverse trend is observed for unsaturated BeSs.

5.2 Comparisons of pore-pressure evolution models

Based on Eq. (1), a dimensionless parameter I is derived by Iverson (2012)

$$I = \frac{H\dot{\gamma}\mu}{k\rho g} \tag{16}$$

where ρ is the debris-flow bulk density. I is only applicable to saturated BeSs since

the depth of the erodible bed H is selected as the length scale of PP diffusion. In this case, De_ζ in Eq. (6) plays a similar role to I. However, the propensity for PP evolution within unsaturated BeSs increases with increasing permeability k and initial water content θ_i (Fig. 8). This tendency is coherent with in-situ observations of natural debris flows (Gabet and Mudd, 2006; McCoy et al., 2012). The effects of permeability and initial water content on the unsaturated BeSs cannot be obtained by I. Furthermore, De_ζ, which indicates the ratio of pore-pressure diffusion to particle deformation timescales, has a clearer physical rationale than I.

5.3 Correlation between pore-pressure evolution and erosion type

Based on a limit equilibrium analysis, Iverson (2012) shows that the erosion rate E of a BeS obeys

$$E = \frac{\tau_f - \tau_b}{\rho u_d} \tag{17}$$

where u_d is the debris-flow velocity, τ_f is the shear stress raised by the debris flow across the bed–flow interface and τ_b is the frictional stress of the BeS. Similar equations for the erosion rate have been proposed by Fraccarollo and Capart (2002), Sovilla et al. (2006) and Medina et al. (2008). These equations for erosion rate presume that the shear tractions and the debris velocities at the interface between the flow and bed are discontinuous. This permits the mass density to remain continuous across the interface and the velocity of erosion of the interface is related to the difference in the flow velocity across the interface. Note that Jenkins and Berzi (2016) presume that the pressure, rather than the shear stress, is discontinuous at the interface.

The flow-front velocity on a BeS is approximately steady, inferred from the laboratory observations of Iverson et al. (2011), de Haas and van Woerkom (2016), and Zheng et al. (2021c). The shear stress of debris flow, τ_f, is approximately equal to the stress arising from the downslope gravity $f_g = \rho g h_d \sin\alpha$, where h_d is the depth of a debris flow. This equation can also be obtained by another derivative approach. The turbulent basal resistance of debris flow is given by (Hungr and McDougall, 2009)

$$\tau_f = \frac{\rho g u_d^2 n_c^2}{h_d^{1/3}} \tag{18}$$

where n_c is the Manning roughness. By making use of the Manning equation, u_d is expressed as

$$u_d = \frac{1}{n_c} h_d^{2/3} (\sin\alpha)^{1/2} \tag{19}$$

Substituting Eq. (19) into Eq. (18) yields the same expression as the stress arising from the downslope gravity f_g. τ_b obeys a Coulomb friction law:

$$\tau_b = \rho g h_d (\tan\varphi_b \cos\alpha - L) \tag{20}$$

where φ_b is the friction angle of BeS and the liquefaction ratio of the sediment bed L is equal to the PP divided by the total stress of a debris flow.

The predictions of Eq. (17) can be compared with erosion rates measured in large-scale experiments in which BeSs with various water contents θ_i are overridden by debris flows (Iverson et al., 2011). Applicable parameter values in these experiments are $\tan\varphi_b$=0.84, g=9.81 m/s^2, $h_d \approx$0.2 m, α=31°, and $u_d \approx$12 m/s. Assigning these values to Eqs. (17) and (20) yields a graph of E as a function of L, as

shown in Fig. 10. The reported erosion rates of 0.05–0.10 m/s for BeSs with initial water contents $\theta_i > 0.22$ are consistent with the predicted erosion rates of 0.05–0.13 m/s when L ranges from about 0.5 to 1.0 that are typically measured in experimental wet BeSs. Experimental erosion rates are smaller than 0.004 m/s for relatively dry BeSs and these values are also consistent with calculated values when L is approximately 0.25. In addition, BeSs are kept in the immobile condition when $L<0.2$, at which the erosion rate decreases to zero.

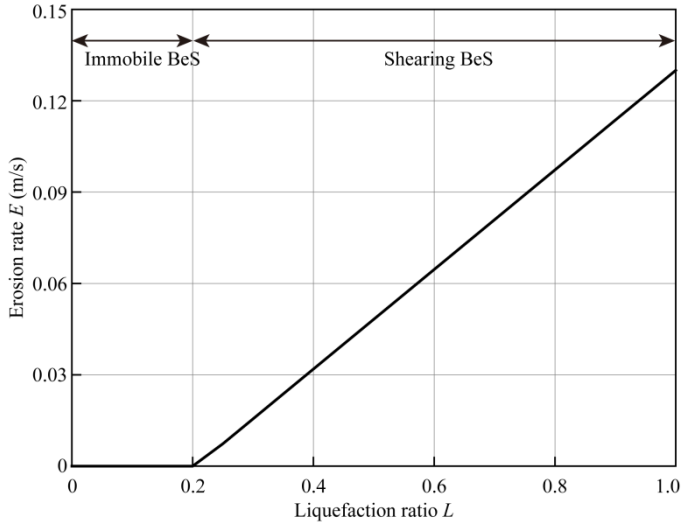

Figure 10. Predicted erosion rates E as a function of the liquefaction ratio L of bed sediment, calculated from Eq. (17). Parameter values are taken from debris-flow erosion experiments of Iverson et al. (2011): $\tan\varphi_b$=0.84, g=9.81 m/s^2, $h_f \approx$0.2 m, α=31°, and $u_d \approx$12 m/s.

BeSs are considered to remain immobile when the erosion rates are zero. The PP developed within a saturated BeS is equal to the basal flow pressure of a debris flow as discussed in section 3.1. The beds composed of silty sands have a stronger tendency to be entrained by debris flow than those of gravels due to the higher

frictional resistance of gravels indicated by Eq. (17) (Zheng et al., 2021a). By contrast, the reverse tendency holds for unsaturated BeSs. The depth of PP diffusion in gravels is larger than that of silty sands as indicated by Eq. (14), leading to a reduction in the effective stress of gravel beds and therefore a reversed tendency.

BeSs are sheared by debris flows when the erosion rates are larger than zero. The erosion rate of a BeS increases with increasing liquefaction ratio according to Eq. (17). A low liquefaction ratio occurs when PP generated by diffusion from basal fluid pressure of a debris flow and shear contraction of the BeS are weak. As a result of a small liquefaction ratio and erosion rate, the debris grains are entrained by progressive scouring in a grain-by-grain manner starting from the top surface of the BeS (Fig. 1a). This situation is applicable to saturated gravel beds due to their high diffusivity, and unsaturated silty sands because of a low penetration depth of pore fluids. Progressive scour is experimentally observed for dry beds formed primarily of silts and sands (de Haas and van Woerkom, 2016; Zheng et al., 2021c).

By contrast, a large PP develops and a high liquefaction ratio occurs when diffusion from basal fluid pressure of a debris flow or shear contraction of the BeS is strong. As a result of high liquefaction and erosion rates, the debris grains within the BeS are entrained by mass flow (Fig. 1b). This situation is appropriate for unsaturated gravels due to a large penetration depth of pore fluid diffusion by Eq. (8) and saturated silty sands due to a small diffusion by Eq. (6). Field observations in Chalk Cliffs basin (McCoy et al., 2012) and experimental observations of wet sediments at large (Iverson et al., 2011) and small (Zheng et al., 2021c) scales show that BeSs with

high water content are eroded by mass movement. Along with mass movement of the BeS (Berger et al., 2011), debris flows monitored at the Illgraben catchment on 1 July 2008 show stepwise removal of debris grains: similar to the experimental observations of Reid et al. (2011) and Zheng et al. (2021c).

5.4 Fluctuating pore pressure in bed sediment

PPs with large magnitude fluctuations are measured in debris flows and near-surface BeSs (McCoy et al., 2012; Kaitna et al., 2016). These fluctuations can be associated with collisional dynamics of coarse grains (Kaitna et al., 2016). They can be generated by positive or negative dilation of debris grains during flow transportation (Iverson and LaHusen, 1989; Iverson and George, 2014). Based on in-situ measurements of sediment entrainment by debris flows, McCoy et al. (2012) infer that the PP fluctuations with a low frequency are generated by gravitational compression of the BeS pores in response to the increasing weight of the overriding flow. The PP fluctuations with high frequency are induced by the shear deformation of the saturated BeS.

To explore the diffusive propagation of the PP fluctuations into the BeS, we simply specify that a sinusoidal pressure fluctuation P' (z = 0, t) is generated at the bed–flow interface. z is the depth of the bed sediment. P' (z = 0, t) is decomposed into discrete frequency components as

$$P'(z=0,\ t)=\sum_{i=1}^{n} A_i \cos(2\pi t f_i) \tag{21}$$

where A_i is the amplitude and f_i is the frequency of the ith frequency component; n is the number of frequency components. P' (z, t) at the bottom of the BeS is considered

to be zero. Using boundary values at the top and bottom of the BeS and initial values given by Eq. (21), the solution to the diffusion equation (Eq. (12)) is given by (Carslaw and Jaeger, 1959)

$$P'(z,\ t) = \sum_{i=1}^{n} A_i \exp\left(-z\sqrt{\frac{\pi f_i}{D}}\right)\cos\left(2\pi t f_i - z\sqrt{\frac{\pi f_i}{D}}\right) \quad (22)$$

The exponential expression in Eq. (22) controls the attenuation that a particular frequency component of P' (z = 0, t) experiences when it penetrates into the BeS. The cosine expression regulates the phase shift of a particular frequency component.

As shown in Fig. 11, pressure fluctuations attenuate during propagation into the BeS. This attenuation depends on the characteristic frequency f_i and diffusion coefficient D. Little attenuation is present for pressure fluctuations with a large diffusion and a low frequency. However, it is significant for pressure fluctuations with a small diffusion and a high frequency. With f_i = 0.1 Hz, pressure fluctuation is reduced by 84% at a depth of 0.02 m for $D = 10^{-4}$ m^2/s. The depth of 0.2 m exhibits the same attenuation for $D = 10^{-2}$ m^2/s. Thus, the depth of pressure fluctuation into silty sands is much smaller than that of gravels at the same specific frequency. From the exponential term, the depth of the BeS required to decrease the amplitude of a particular frequency component of P' (z = 0, t) by 1/e can be written as

$$h_e = \sqrt{\frac{D}{\pi f_i}} \quad (23)$$

This analysis highlights the diffusive nature by which the PP fluctuations propagate and the resulting diffusion-dependent amplitude attenuation. These factors severely limit the depth of silty sand with low permeability to which large-magnitude pressure

fluctuations can reduce Coulomb frictional resistance and intensify erosion according to Eq. (17). The attenuation regularity of the PP fluctuation shown in Fig. 11 is applicable to both saturated and unsaturated BeSs.

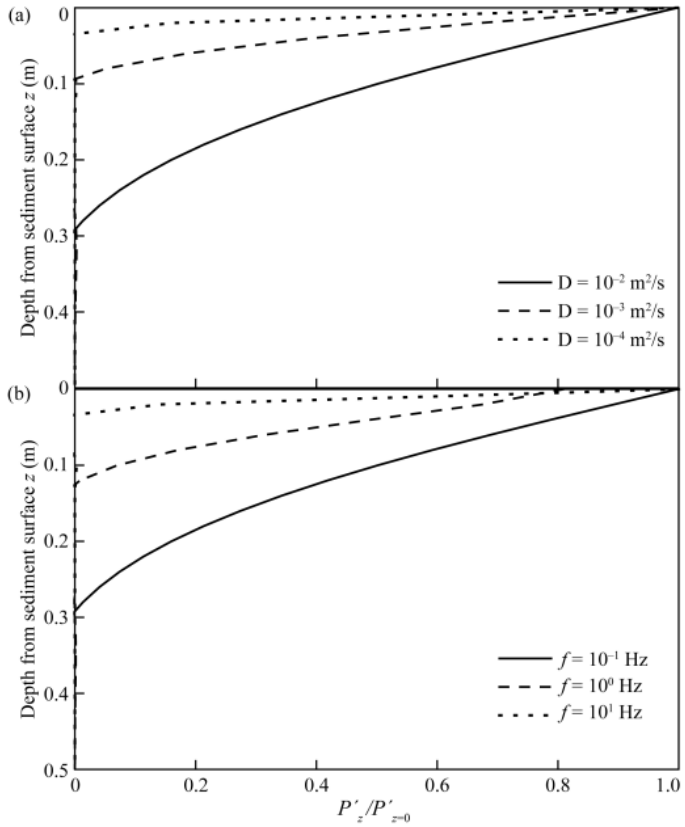

Figure 11. Depth profiles of PP resulting from sinusoidal pressure fluctuations with various characteristics: (a) diffusions into BeS with a characteristic frequency of 0.1 Hz and (b) frequencies of fluctuation with a diffusion coefficient of 10^{-2} m^2/s. The depth to which surface pressure fluctuations penetrate the BeS increases as the diffusion increases or as the frequency of fluctuation decreases.

5.5 Implication

Our models can be used to interpret the feedback of PP on the flow momentum during debris-flow entrainment. The flow resistance quantified in Eq. (17) is the shear traction exerted by the underlying BeS. Little bed resistance is developed to inhibit

flow acceleration during erosion of BeS for a nearly liquefied Coulomb bed. Thus, the mass and velocity of a flow that liquefies its bed can significantly increase (Iverson et al., 2011). However, if significant PP diffusion from the flow into the BeS occurs, it brings about a decrease in the fluid pressure of the flow and enhances the basal resistance. Consequently, a significant reduction of the velocity is observed when flows override the BeS (de Haas and van Woerkom, 2016; Zheng et al., 2021c).

In this study, bed state is classified as immobile and shearing to analyze PP generation from the debris flow and the bed. In practice, BeS can transition from immobile to shearing during entrainment because frictional stress in Eq. (20) decreases with increasing PP. This means that PP development is complex owing to the changes of bed state, water content and permeability.

Our model provides a general formulation of mass bulking by debris flows and can be considered by large scale or laboratory debris-flow monitoring test sites. The correlation between the slope angle, the thickness, permeability and water content of the erodible bed and PP evolution as well as erosion rate are quantified. Furthermore, the effects of the velocity, volume, grain composition and density of flows on the erosion rate and flow momentum can be further inferred from this model.

6. Conclusions

We present a general formulation describing pore-fluid pressure (PP) evolution within bed sediment (BeS) under immobile and shearing conditions in response to debris flow loading, which is applicable to both saturated and unsaturated beds. The formulation is used to examine the conditions and processes under which PP evolves

necessary to liquefy the BeS, resulting in significant mass bulking and thus momentum growth during debris-flow entrainment.

It is found that the relative degree of drainage expressed by a specific Deborah number De_ζ plays an important role in the evolution of PP during flow loadings. Here, $De_\zeta=t_\zeta/t_0$ expresses the ratio between the timescale of relaxation for PP diffusion across the bed layer and the timescale of grain deformation. De_ζ is approximately zero for an immobile BeS with $\nabla \cdot \mathbf{u}_s = 0$ and PP within the BeS is generated from the basal fluid pressure of debris flow. PP of a saturated BeS under immobile conditions is equal to the fluid pressure at the bottom of the flow due to a non-flux basal boundary, while PP of an unsaturated BeS is lower than the value of flow pressure. Pore-pressure diffusion from debris flows into unsaturated beds increases with increasing permeability and water content of the bed. When $De_\zeta>1$and $\nabla \cdot \mathbf{u}_s < 0$, the shearing sediment presents effectively undrained behavior and a high propensity for large PP development. This situation is applicable to saturated BeSs with a low permeability or a large shear velocity as well as unsaturated BeSs with a high permeability and a large water content. When $De_\zeta<1$ and $\nabla \cdot \mathbf{u}_s < 0$, the shearing sediment presents drained behavior and a high tendency to develop weak PP. This situation is appropriate for saturated BeSs with a high permeability and a small shear velocity as well as unsaturated BeSs with a low permeability or a small water content.

When $De_\zeta>1$, a significant PP and liquefaction ratio occur for the overridden BeS. As a result of high liquefaction ratio and erosion rate, the debris grains within the BeS are entrained by mass flow. By contrast, when $De_\zeta<1$, a low liquefaction ratio of the

BeS arises because of the weak PP. Debris grains are entrained by progressive grain-by-grain scour on the surface of the BeS due to a small erosion rate. The attenuation of pore-pressure fluctuation increases with increasing characteristic frequency or decreasing diffusion coefficient.

Acknowledgements

We acknowledge funding from the Natural Science Foundation of China (No. 42007252 and41731283). We thank Liran Goren and Bo Li for their discussion on the erosion pattern of debris flows.

Conflicts of Interest

The authors declare that they do not have any conflict of interest.

Appendix A: Diffusion equation of pore pressure

Mass and momentum conservation laws are adopted for the development of a pore pressure diffusion equation in Eq. (1).

Let ϕ be the porosity, t the time, and ρ_f and ρ_s the mass densities of the pore fluid and debris grains, respectively. $\mathbf{u_f}$ and $\mathbf{u_s}$ are the velocities of the fluid and grains, respectively. First, mass conservation equations are written for the debris grains and the pore fluid:

$$\frac{\partial[(1-\phi)\rho_s]}{\partial t} + \nabla \cdot [(1-\phi)\rho_s \mathbf{u_s}] = 0 \tag{A1}$$

$$\frac{\partial[\phi\rho_f]}{\partial t} + \nabla \cdot [\phi\rho_f \mathbf{u_f}] = 0 \tag{A2}$$

where $\nabla\cdot$ is a divergence operator with respect to grains or fluid advective processes.

The velocities are considered at a representative scale for Darcy's law; that is, they are defined for mesoscopic volumes containing at least a few grains. The fluid specific discharge $\phi(\mathbf{u_f} - \mathbf{u_s})$ corresponding to the Darcy velocity in the saturated zone (Iverson, 1997) is written as

$$\phi(\mathbf{u_f} - \mathbf{u_s}) = -\frac{k}{\mu}\nabla P \tag{A3}$$

where k is the permeability of the BeS and μ is the viscosity of pore fluid; P is the excess (over hydrostatic) fluid pressure.

Considering the stress magnitude is smaller than 100 kPa for a typical debris flow (Iverson, 1997), the densities of the debris grains and pore fluid are assumed to be constant. Then, Eqs. (A1) and (A2) reduce to:

$$-\frac{\partial \phi}{\partial t}-\nabla \cdot (\phi \mathbf{u_s})+\nabla \cdot \mathbf{u_s}=0 \tag{A4}$$

$$\frac{\partial \phi}{\partial t}+\nabla \cdot (\phi \mathbf{u_f})=0 \tag{A5}$$

Rearranging Eq. (A4), we obtain

$$\nabla \cdot \mathbf{u_s}=\frac{1}{1-\phi}\frac{d\phi}{dt} \tag{A6}$$

Combining Eqs. (A3), (A4) and (A5) yields an equation that governs the non-equilibrium pore pressure *P*:

$$\nabla \cdot \mathbf{u_s}=\nabla \cdot \frac{k}{\mu}\nabla P \tag{A7}$$

When $\nabla \cdot \mathbf{u_s}>0$, the flows into the increasing pore volume and pore fluid depressurizes. A negative PP can be generated along with the dilation of the BeS. This phenomenon is often observed in dense BeSs. The regulation of landslide motion by negative PP has been interpreted by Iverson (2005) and is not discussed here. When $\nabla \cdot \mathbf{u_s}<0$, the pore volume collapses and pore fluid pressurizes during entrainment. In practice, natural torrent deposits are commonly loose and a positive PP arises accompanied by the contraction of BeS (Sassa and Wang, 2005).

The changes in porosity ϕ of BeSs are associated with changes in the mean effective normal stress, σ_e, and the shear deformation, γ (see the deduction in Appendix B):

$$\frac{1}{1-\phi}\frac{d\phi}{dt}=\dot{\gamma}\tan\varphi-C\frac{d\sigma_e}{dt} \tag{A8}$$

where $\dot{\gamma}$ is the shear rate of the BeS; $\sigma_e = \sigma - P$ is equal to the difference between the total normal stress σ and P.

Appendix B: Dilation rate

The dilation rate postulated by Iverson and George (2014) is controlled by two mechanical phenomena that modify the solid volume fraction m ($m = 1-\phi$): changes in σ_e that cause changes of the pore space due to bulk compressibility of the bed sediment, and changes in mixture shear strain due to dilatancy. These two phenomena are assumed to be independent; however, they are influenced by other variables such as pore pressure. The total rate of change of m is defined as

$$\frac{dm}{dt} = \frac{\partial m}{\partial \sigma_e}\frac{d\sigma_e}{dt} + \frac{\partial m}{\partial \gamma}\dot{\gamma} \tag{B1}$$

where $\dot{\gamma} = d\gamma/dt$ is the associated shear rate. For a typical debris flow in the field, the bulk expansion or compression of bed sediment caused by changes in σ_e is almost entirely induced by changes in pore volume rather than changes in the densities of the debris grains and interstitial fluid. The debris compressibility C can thus be obtained using a relationship commonly employed in soil mechanics (Bear, 1972):

$$C = \frac{1}{m}\frac{\partial m}{\partial \sigma_e} \tag{B2}$$

The evolving dilatancy angle φ is estimated as

$$\tan\varphi = \frac{1}{V}\frac{\partial V}{\partial \gamma} = \frac{1}{m}\frac{\partial m}{\partial \gamma} \tag{B3}$$

where V is the volume of the bed sediment.

Combine Eq. (B3) with Eqs. (B1) and (B2) to obtain a definition of φ in terms of rates:

$$\dot{\gamma}\tan\varphi = C\frac{d\sigma_e}{dt} - \frac{1}{m}\frac{dm}{dt} \tag{B4}$$

Thus, the total dilation rate $(-1/m)\ dm/dt$ describes the portion of the total dilation rate caused by changes in the mean effective stress, $C(d\sigma_e/dt)$, and any non-zero shear rate, $\dot{\gamma}$.

Appendix C: Infiltration depth

The Green–Ampt model (Green and Ampt, 1911) assumes a homogeneous sediment profile and a uniform distribution of initial soil water content. As shown in Fig. S1, the model assumes that a wetting front is present in the soil profile, and that the front separates the profile into an upper saturated zone and a lower unsaturated zone where the water content is kept at the initial soil value (Chen and Young, 2006). Lateral movement of soil water content is neglected, even in cases where the bed sediment is no longer perpendicular to the gravity vector.

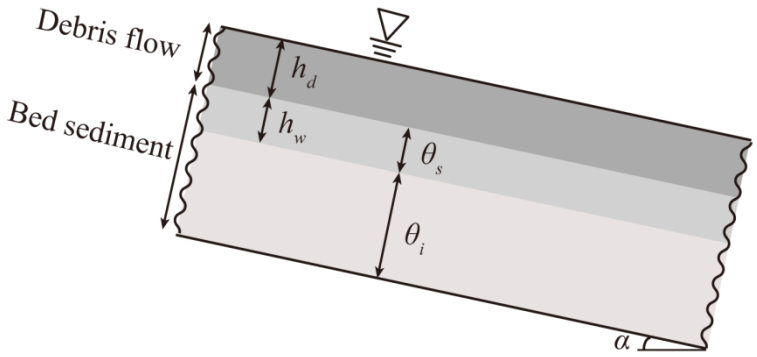

Figure S1. Sketch of the vertical infiltration of a debris flow into a bed sediment.

On the basis of Darcy's law, the Green–Ampt model for the sloping sediment infiltrated by the debris flow can be expressed in the following form:

$$i = K_e\frac{h_w\cos\alpha + s_f + h_d}{h_w} \tag{C1}$$

where i is the infiltration rate and K_e is the effective saturated hydraulic conductivity.

Here, K_e is approximated as the saturated hydraulic conductivity K. h_w is the wetting front depth in the direction normal to the bed sediment, s_f is the wetting front matric potential. h_d is the depth of debris flow and $h_w\cos\alpha$ represents gravity head at the wetting front.

The cumulative infiltration depth in the normal direction, N, can be expressed as

$$N = h_w(\theta_s - \theta_i) \tag{C2}$$

where θ_s and θ_i are the saturated and initial water contents of the BeS, respectively.

Taking the derivative of N with respect to time t and substituting into Eq. (C1) yields

$$\frac{dh_w}{dt} = \frac{K}{\theta_s - \theta_i}\frac{h_w\cos\alpha + s_f + h_d}{h_w} \tag{C3}$$

Integrating Eq. (C3) with respect to time:

$$t = \frac{(\theta_s - \theta_i)}{K\cos\alpha}\left[h_w - \frac{(s_f + h_d)}{\cos\alpha}\mathrm{In}\frac{h_w\cos\alpha + s_f + h_d}{s_f + h_d}\right] \tag{C4}$$

Combining Eqs. (C2) and (C4) yields the simplified form

$$Kt\cos\alpha = N - \frac{S\theta}{\cos\alpha}\mathrm{In}\left[1 + \frac{N\cos\alpha}{S\theta}\right] \tag{C5}$$

where $S = s_f + h_d,\ \theta = \theta_s - \theta_i$.

Let us define the characteristic magnitudes of the variables in the equation as $\hat{t} = t/t_c,\ \hat{N} = \frac{1}{\cos\alpha}\frac{N}{S\theta},\ t_c = \frac{S\theta}{K}$. Eq. (C5) is reduced to

$$\hat{t} = \hat{N} - \frac{1}{\cos^2\alpha}\mathrm{In}\left[1 + \hat{N}\cos^2\alpha\right] \tag{C6}$$

The non-dimensionalized $\hat{N}$ is approximately proportional to the non-dimensionalized $\hat{t}$, as shown in Fig. S2. That is $\hat{N} \approx \beta\hat{t}$ and β varies from

1.08–1.10 for different α. β = 1.0 is adopted considering the propensity for PP generation is derived. Hence, the dimensional infiltration depth N can be simplified as

$$N = Kt \tag{C7}$$

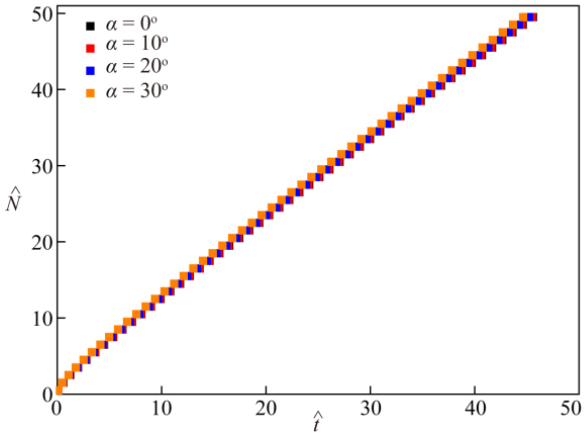

Figure S2. Cumulative infiltration depth versus slope angle and time during infiltration.

Notation

A_i	amplitude of the ith frequency component
BeS	bed sediment
C	compressibility of the bulk bed sediment
D	diffusion coefficient
d_g	characteristic particle diameter
De_d	Deborah number of grain
De_ζ	Deborah number of bed sediment
E	erosion rate of bed sediment
f_i	frequency of the ith frequency component
g	gravitational acceleration
h	depth of PP diffusion
h_d	debris-flow depth
h_i	infiltration depth in the unsaturated bed
h_w	wetting front depth
H	depth of the erodible bed
i	hydraulic gradient
k	permeability of the bed sediment
K	saturated hydraulic conductivity
K_e	effective saturated hydraulic conductivity
l	length scale of PP diffusion
L	liquefaction ratio of the sediment bed

m	solid volume fraction
n	number of frequency components
N	cumulative infiltration depth
n_c	Manning roughness
P	excess (over hydrostatic) fluid pressure
PP	pore-fluid pressure
P_i	transient excess pore pressure
P_e	pore pressure at the bottom of a debris flow
P_u	pore pressure diffused from the top of the debris flow
P_w	pore pressure diffused from the wetting front
P'	pore-pressure fluctuation
s_f	wetting front matric potential
t	time
t_0	timescale of particle deformation
t_d	timescale for pore-pressure diffusion across a single particle
t_ζ	timescale of PP diffusion over a saturated bed sediment
u_d	velocity of debris flow
$\mathbf{u_f}$	pore-fluid velocity
$\mathbf{u_s}$	bed-grain velocity
u_s	bed-grain velocity in the shear direction
u_0	velocity of sediment for characterizing the timescale of particle deformation
V	volume of the bed sediment

z	depth of the bed sediment
μ	viscosity of pore fluid
α	slope of bed sediment
β	proportionality coefficient
θ	difference between the saturated water content and initial water content
θ_s	saturated water content of bed sediment
θ_i	initial water content of bed sediment
ρ	debris-flow density
ρ_f	mass density of pore fluid
ρ_s	mass density of debris grains
σ	total normal stress
σ_e	mean effective normal stress
γ	shear deformation of bed sediment
$\dot{\gamma}$	shear rate of bed sediment
λ_n	eigenvalues
τ_f	shear stress raised by the debris flow
τ_b	frictional stress of the bed sediment
φ	dilatancy angle of bed sediment
φ_b	friction angle of bed sediment
ϕ	porosity of bed sediment
$\nabla\cdot$	divergence operator

References

An H, Ouyang C, Wang D. 2021. A new two-phase flow model based on coupling of the depth-integrated continuum method and discrete element method. *Computers & Geosciences* **146**: 104640.

Bear J. 1972. Dynamics of fluids in porous media. New York, NY: Dover.

Berger C, McArdell BW, Fritschi B, Schlunegger F. 2010. A novel method for measuring the timing of bed erosion during debris flows and floods. *Water Resources Research* **46**: W02502.

Berger C, McArdell BW, Schlunegger F. 2011. Direct measurement of channel erosion by debris flows, Illgraben, Switzerland. *Journal of Geophysical Research* **116**: F01002.

Breien H, De Blasio FV, Elverhøi A, Høeg K. 2008. Erosion and morphology of a debris flow caused by a glacial lake outburst flood, western Norway. *Landslides* **5**: 271–280.

Berti M, and Simoni A. 2005. Experimental evidences and numerical modelling of debris flow initiated by channel runoff. *Landslides* **2**: 171–182.

Carslaw H, Jaeger J. 1959. Conduction of Heat in Solids, pp. 264, Oxford Univ. Press, Oxford, U. K.

Chen M, Tang C, Zhang X, Xiong J, Chang M, Shi Q, Wang F, Li M. 2021. Quantitative assessment of physical fragility of buildings to the debris flow on 20 August 2019 in the Cutou gully, Wenchuan, southwestern China. *Engineering Geology* **293**: 106319.

Chen L, Young M. 2006. Green-Ampt infiltration model for sloping surfaces. *Water Resources Research,* **42**: W07420.

de Haas T, van Woerkom T. 2016. Bed scour by debris flows: experimental investigation of effects of debris-flow composition. *Earth Surface Processes and Landforms* **41**: 1951–1966.

de Haas T, Braat L, Leuven JR, Lokhorst IR, Kleinhans MG. 2015. Effects of debris flow composition on runout, depositional mechanisms, and deposit morphology in laboratory experiments. *Journal of Geophysical Research: Earth Surface* **120**: 1949–1972.

Fraccarollo L, Capart H. 2002. Riemann wave description of erosional dam-break flows. *Journal of Fluid Mechanics* **461**: 183–228.

Gabet EJ, Mudd SM. 2006. The mobilization of debris flows from shallow landslides. *Geomorphology* **74**: 207–218.

Goren L, Aharonov E, Sparks D, Toussaint R. 2010. Pore pressure evolution in deforming granular material: A general formulation and the infinitely stiff approximation. *Journal of Geophysical Research* **115**: B09216.

Green WH, Ampt GA. 1911. Studies on soil physics. *Journal of Agricultural Science* **4(1)**: 1–24.

Hsu L, Dietrich WE, Sklar LS. 2008. Experimental study of bedrock erosion by granular flows. *Journal of Geophysical Research* **113**: F02001.

Hungr O, Evans SG. 2004. Entrainment of debris in rock avalanches: An analysis of a long run-out mechanism. *GSA Bulletin* **116(9-10)**: 1240–1252.

Hungr O, McDougall S. 2009. Two numerical models for landslide dynamic analysis. *Computers and Geosciences* **35**: 978–992.

Hungr O, McDougall S, Bovis M. 2005. Entrainment of material by debris flows. In Debris-flow hazards and related phenomena, (Ed. Jakob, M., & Hungr, O.), pp. 135–158, Springer, Berlin.

Hutchinson JN, Bhandari RK. 1971. Undrained loading, a fundamental mechanism of mudflows and other mass movements. *Géotechnique* **21**: 353–358.

Iverson RM, LaHusen RG. 1989. Dynamic pore-pressure fluctuations in rapidly shearing granular materials. *Science* **246(4931)**: 796–799.

Iverson RM. 1993. Differential equations governing slip-induced pore-pressure fluctuations in a water-saturated granular medium. *Mathematical Geology*, **25(8):** 1027–1048.

Iverson RM. 1997. The physics of debris flows. *Reviews of Geophysics* **35(3)**: 245–296.

Iverson RM. 2000. Landslide triggering by rain infiltration. *Water Resources Research* **36**: 1897–1910.

Iverson RM. 2005. Regulation of landslide motion by dilatancy and pore pressure feedback. *Journal of Geophysical Research* **110**: F02015.

Iverson RM, Reid ME, Logan M, LaHusen RG, Godt JW, Griswold JP. 2011. Positive feedback and momentum growth during debris-flow entrainment of wet bed sediment. *Nature Geoscience* **4**: 116–121.

Iverson RM. 2012. Elementary theory of bed-sediment entrainment by debris flows and avalanches. *Journal of Geophysical Research* **117**: F03006.

Iverson RM, George DL. 2014. A depth-averaged debris-flow model that includes the effects of evolving dilatancy. I. Physical basis. *Proceedings of the Royal Society A Mathematical Physical and Engineering Sciences* **470**: 20130819.

Iverson RM, Ouyang C. 2015. Entrainment of bed material by Earth-surface mass flows: Review and reformulation of depth-integrated theory. *Reviews of Geophysics* **53(1):** 27–58.

Jenkins JT, Berzi D. 2016. Erosion and deposition in depth-averaged models of dense, dry, inclined, granular flows. *Physical Review E* **94**: 052904.

Kaitna R, Palucis MC, Yohannes B, Hill KM, Dietrich WE. 2016. Effects of coarse grain size distribution and fine particle content on pore fluid pressure and shear behavior in experimental debris flows. *Journal of Geophysical Research: Earth Surface* **121**: 415–441.

Major JJ. 2000. Gravity-driven consolidation of granular slurries: implications for debris-flow deposition and deposit characteristics. *Journal of Sedimentary Research,* **70**: 64–83.

Mangeney A. 2011. Geomorphology: Landslide boost from entrainment. *Nature Geoscience* **4**: 77.

McCoy SW, Kean JW, Coe JA, Tucker GE, Staley DM, Wasklewicz TA. 2012. Sediment entrainment by debris flows: In situ measurements from the headwaters of a steep catchment. *Journal of Geophysical Research* **117**: F03016.

McGuire LA, Rengers FK, Kean JW, Staley DM. 2017. Debris flow initiation by runoff in a recently burned basin: Is grain-by-grain sediment bulking or en masse failure to blame?, *Geophysical Research Letters* **44**: 7310–7319.

Medina V, Hürlimann M, Bateman A. 2008. Application of FLATModel, a 2D finite volume code, to debris flows in the northeastern part of the Iberian Peninsula. *Landslides* **5**: 127–142.

Navratil O, Liébault F, Bellot H, Travaglini E, Theule J, Chambon G, Laigle D. 2013. High-frequency monitoring of debris-flow propagation along the Réal Torrent, Southern French Prealps. *Geomorphology* **201**: 157–171.

Osswald T. 1998. Polymer processing fundamentals, Hanser Gardner, Cincinnati, Ohio.

Pierson TC. 1980. Erosion and deposition by debris flows at Mt. Thomas, North Canterbury, New Zealand. *Earth Surface Processes and Landforms* **5**: 227–247.

Pudasaini SP. 2012. A general two-phase debris flow model. *Journal of Geophysical Research* **117**: F03010.

Pudasaini SP, Krautblatter M. 2021. The mechanics of landslide mobility with erosion. *Nature Communications* **12(1):** 1–15.

Reid ME, Iverson RM, Logan M, LaHusen RG, Godt J, Griswold J. 2011. Entrainment of bed sediment by debris flows: results from large-scale experiments. In Debris-Flow Hazards Mitigation, Mechanics, Prediction, and Assessment: Proceedings of 5th International Conference, Padua, Italy; 367–374.

Santi PM, Higgins JD, Cannon SH, Gartner JE. 2008. Sources of debris flow material in burned areas. *Geomorphology* **96**: 310–321.

Sassa K. 1985. The mechanism of debris flows, in Proceedings of the Eleventh International Conference on Soil Mechanics and Foundation Engineering, pp. 1173–1176, Balkema, Rotterdam, Netherlands.

Sassa K, Wang GH. 2005. Mechanism of landslide-triggered debris flows: Liquefaction phenomena due to the undrained loading of torrent deposits. In Debris-Flow Hazards and Related Phenomena; Springer: Berlin/Heidelberg, Germany, 81–104.

Scheidl C, Rickenmann D. 2010. Empirical prediction of debris-flow mobility and deposition on fans. *Earth Surface Processes and Landforms* **35**: 157–173.

Sovilla B, Burlando P, Bartelt P. 2006. Field experiments and numerical modeling of mass entrainment in snow avalanches. *Journal of Geophysical Research* **111**: F03007.

Takahashi T, Nakagawa H, Harada T, Yamashiki Y. 1992. Routing debris flows with particle segregation. *Journal of Hydraulic Engineering* **118**: 1490–1507.

Takahashi T. 2007. Debris flow: mechanics, prediction and countermeasures. Taylor and Francis, London.

Tang C, van Asch TWJ, Chang M, Chen G, Zhao X, Huang X. 2012. Catastrophic debris flows on 13 August 2010 in the Qingping area, southwestern China: The combined effects of a strong earthquake and subsequent rainstorms. *Geomorphology* **139–140**: 559–576.

Terzaghi, K. (1943). Theoretical soil mechanics. John Wiley.

Theule J, Liébault F, Laigle D, Loye A, Jaboyedoff M. 2015. Channel scour and fill by debris flows and bedload transport. *Geomorphology* **243**: 92–105.

Tiranti D, Bonetto S, Mandrone G. 2008. Quantitative basin characterisation to refine debris-flow triggering criteria and processes: an example from the Italian Western Alps. *Landslides* **5(1)**: 45–57.

Wang Y, Cheng Q, Yuan Y, Wang J, Qiu Y, Yin B, Shi A, Guo Z. 2020. Emplacement mechanisms of the Tagarma rock avalanche on the Pamir-western Himalayan syntaxis of the Tibetan Plateau, China. *Landslides* **17**: 527–542.

Zheng H, Shi Z, Peng M, Yu S. 2018. Coupled CFD-DEM model for the direct numerical simulation of sediment bed erosion by viscous shear flow. *Engineering Geology* **245**: 309–321.

Zheng H, Shi Z, Hanley KJ, Peng M, Guan S, Feng S. Chen K. 2021a. Deposition characteristics of debris flows in a lateral flume considering upstream entrainment. *Geomorphology* **394(1160)**: 107960.

Zheng H, Shi Z, Shen D, Peng M, Hanley KJ, Ma C, Zhang L. 2021b. Recent advances in stability and failure mechanisms of landslide dams. *Frontiers in Earth Science* **9**: 659935.

Zheng H, Shi Z, Yu S, Fan X, Hanley KJ, Feng S. 2021c. Erosion mechanisms of debris flow on the sediment bed. *Water Resources Research* **57(12)**: WR030707.

Zheng H, Shi Z, de Haas T, Shen D, Hanley KJ, Li Bo. 2022. Characteristics of the impact pressure of debris flows. *Journal of Geophysical Research: Earth Surface*: e2021JF006488.